Roles of Physical Aging on Crystallization Kinetics and Induction Period of Poly(L-lactide)

Pengju Pan, Zhichao Liang, Bo Zhu, Tungalag Dong, and Yoshio Inoue*

Department of Biomolecular Engineering, Tokyo Institute of Technology, 4259-B-55 Nagatsuta, Midori-ku, Yokohama 226-8501, Japan

Received June 27, 2008; Revised Manuscript Received August 25, 2008

ABSTRACT: Effects of physical aging temperatures (T_a 40 and 50 °C) and times (t_a 0−840 h) on the crystallization kinetics as well as induction periods of poly(L-lactide) (PLLA) have been studied by differential scanning calorimetry (DSC) and time-resolved Fourier transform infrared (FTIR) spectroscopy. The crystallization rate of PLLA increases considerably after the physical aging process. According to the DSC analysis, the crystallization temperature (T_c) of the nonisothermal crystallization and the crystallization half-time ($t_{1/2}$) in the isothermal crystallization decrease nearly logarithmically with t_a in the investigated t_a region. With increasing T_a, both the T_c and $t_{1/2}$ values decrease. Polarized optical microscopy (POM) observation revealed that the nucleation of PLLA becomes faster and the nucleation density increases significantly with physical aging. Besides, the crystallization induction period of PLLA shortens with aging. It was found that the FTIR spectral intensity changes of the conformation-sensitive and the pure crystalline bands are not synchronous in the crystallization process. FTIR results suggest that the conformational rearrangement from *gg* to *gt* conformers likely occurs during the crystallization induction period of PLLA. It was concluded that the aging effect on the crystallization behavior of PLLA could be correlated with the chain conformational and microstructural rearrangements that occurred during the aging process.

Introduction

Poly(L-lactide) (PLLA), as a biodegradable polymer, has attracted considerable interest from both fundamental and practical perspectives because it can be synthesized from renewable resources and is thus environmentally and economically appropriate. Since its degradation products are nontoxic and bioresorbable, this polymer is one of the selected few candidates for use in biomedical fields, such as implant materials, surgical sutures, and controlled drug delivery systems.[1] Furthermore, the attributes of biodegradability, producibility from renewable resources, good mechanical properties, and versatile fabrication processes make it a promising material for many disposable products as well as for the traditional applications where common thermoplastics are employed.[1]

In general, upon quenching an amorphous polymer from above the glass transition temperature (T_g) into the glassy state, the chain mobility decreases significantly and the molecules are unable to reach an equilibrium packing density and conformational structure with respect to a given temperature. The process of relaxation toward equilibrium is commonly referred to as physical aging.[2] It has been widely reported that physical aging can lead to changes in the physical properties of polymers such as yield strength, tensile modulus, gas barrier resistance, etc.[3−6] Therefore, the structural recovery and physical aging responses of polymers are important to determine the long-term performance of the material system. In the past few decades, considerable attention has been paid to investigating the physical aging behavior of a variety of polymers.[3−6] As with other biomedical or traditional polymeric materials, PLLA is usually used below T_g (ca. 60 °C), and the physical aging process will inevitably occur during its service life. Therefore, it is of fundamental importance to understand the physical aging behavior of PLLA and its impact on physical properties.

Although the changes in physical properties of materials during physical aging have been correlated with the structural changes taking place, the details of this relationship between structure and properties during physical aging remain somewhat unclear. In a previous paper,[7a] we have reported that the mechanical properties, especially the toughness, of amorphous PLLA are dramatically affected by the physical aging process. The fracture strain in the tensile test decreases from more than 300% to ∼6% during physical aging, accompanied by variation of the fracture mechanism from ductile to brittle. Besides, with employment of in situ Fourier transform infrared (FTIR) spectroscopy and ^{13}C high-resolution solid-state NMR measurements, we have demonstrated that the conformational and microstructural rearrangements of PLLA take place upon physical aging.[7b] These could explain the structure−property relationship for PLLA-based materials to some extent.

Apart from mechanical properties, the crystallization kinetics have also been reported to be dependent on the physical aging process.[6] There has been some argument as to whether the structural changes due to physical aging can persist above T_g and thus changes the rates and mechanism of cold-crystallization. As for poly(ethylene terephthalate) (PET), Mcgonigle et al.[6a] reported that short-term aging accelerated the subsequent crystallization, while long-term aging retarded it. They also invoked two competitive mechanisms, that is, molecular ordering and chain segmental mobility, to explain these effects. However, Lu and Hay[6b] found that physical aging only increased the cold-crystallization rate of PET. Besides the crystallization kinetics, the mechanism for the effect of physical aging on the cold-crystallization process still remains unclear. As we know, the crystallization rate of PLLA is very slow and it is easy to attain an amorphous sample. In this work, we selected PLLA as a model polymer to study the relationship between the physical aging and cold-crystallization processes.

The microstructral formations during the induction period before the start of the major crystallization have been one of the most important research topics in polymer crystallization. Imai et al.[8] have studied the crystallization process of unoriented PET from the glassy state by using small-angle X-ray scattering (SAXS), small-angle neutron scattering (SANS), and wide-angle X-ray diffraction (WAXD). They observed the formation of a

* To whom corresponding should be addressed: tel +81-45-924-5794; fax +81-45-924-5827; e-mail inoue.y.af@m.titech.ac.jp.

10.1021/ma801436f CCC: $40.75
Published on Web 10/10/2008

long-range ordered structure with a size of ~20 nm during the induction period of crystallization. Long-range ordered structure was ascribed to the spinodal decomposition, causing segregation of a rodlike conformation from more random chain conformation. By using in situ WAXD and SAXS measurements, Radhakrishnan and Kaito[9a] also suggested that the PET chains undergo an ordering process in the crystallization induction period; Nogales et al.[9b] found that the long-range ordered structure is developed during the crystallization induction period of two semirigid polymers, poly(ethylene naphthalene) (PEN) and poly(aryl ether ketone ketone) (PEEK). The existence of a transient state or metastable step in polymer crystallization has also been reported by several authors.[10−12] All these studies suggested the formation of more ordered structures at very early stage of crystallization. On the other hand, conformational characteristics of polymer chains during the crystallization induction period of semicrystalline polymers have been studied by FTIR spectroscopy. From in situ detection of the FTIR absorbance change of conformation-sensitive bands, chain conformational changes in the crystallization induction period have been demonstrated for PET, isotactic, and syndiotactic polystyrene, etc.[13]

A great number of studies on PLLA crystallization have been reported, but most of them mainly focused on the crystalline structure and crystallization kinetics. The microstructural and conformational features of PLLA during the induction period before crystal nucleation have hardly been studied. On the other hand, on the basis of X-ray scattering and FTIR measurements, several authors have suggested that formation of local ordering domain[14] and changes of chain conformation[15] occur during the physical aging process of amorphous polymers. It is speculated that the microstructural and conformational rearrangements in the two processes, that is, physical aging and crystallization induction period, could have some connections. Previous studies[16] have reported that FTIR spectrum is highly sensitive to the conformation, crystalline structure, and chain packing of PLLA. In this work, the crystallization induction period of PLLA and its dependence on the physical aging process were investigated by time-resolved FTIR spectroscopy. This is considered to be important for further understanding of the structural and conformational features of polymer during the crystallization induction period as well as physical aging processes.

In this paper, the effects of physical aging on nonisothermal and isothermal crystallization kinetics and on spherulite morphology were investigated. The crystallization induction periods of unaged and aged PLLA were studied by time-resolved FTIR spectroscopy, and the conformational features of PLLA during the crystallization induction period were analyzed. Besides, the mechanism for the physical aging effect on the crystallization behavior was discussed.

Experimental Section

Materials. PLLA sample (M_n = 94 kg/mol, M_w/M_n = 1.52) was kindly supplied by Unitika Co. Ltd. (Kyoto, Japan). The glass transition temperature (T_g) of the sample, which was estimated from the differential scanning calorimetric (DSC) heating curve at 10 °C/min, is ~55 °C. Before use, the sample was purified by precipitation into ethanol from chloroform solution and then was dried in the vacuum oven at 40 °C for 3 days.

The dried PLLA sample was hot-pressed under a pressure of 10 MPa after it was melted at 200 °C for 2 min, followed by quenching to ~23 °C. The as-prepared sample was proven to be amorphous by WAXD and FTIR measurements because of the absence of any diffraction peak and characteristic IR band of the PLLA crystalline phase. The same processing conditions (temperature, time, and pressure) were maintained throughout to ensure reproducibility in the sample preparation.

Measurements. Differential Scanning Calorimeter. The thermal properties of PLLA after physical aging were analyzed on a Pyris Diamond DSC instrument (Perkin-Elmer Japan Co., Yokohama, Japan). The scales of temperature and heat flow at different heating rates were calibrated by use of an indium standard with nitrogen purging. Daily baseline calibrations were performed at each heating rate to eliminate the baseline noise. The aging experiment is similar to the procedure reported previously.[7a]

In the isothermal aging experiments, samples that were to be annealed for times of 6 h or less were weighted and sealed in an aluminum pan and melted at 200 °C for 2 min, followed by a rapid quenching. Afterward, they were annealed at 40 (or 50) °C in the calorimeter. Because it is impractical to use the instrument as an oven for longer annealing times, for annealing times larger than 6 h, the samples were transferred, immediately after quenching, into an oven controlled at 40 or 50 °C. After annealing for a certain time, the samples were quickly sealed in an aluminum pan for DSC measurement. To study the nonisothermal cold-crystallization behavior, all the aged samples were scanned from 0 to 200 at 10 °C/min. For the isothermal cold-crystallization experiment, the samples were rapidly heated to 90 °C (or 75 °C) at 100 °C/min and were held for crystallization. No discontinuity was observed between the results obtained for the samples annealed for less than and greater than 6 h, indicating that the two annealing procedures (in the calorimeter and oven) are equivalent.

Fourier Transform Infrared Spectroscopy. Time-resolved FTIR measurements in the transmission mode were performed on an AIM-8800 automatic infrared microscope (Shimadzu, Kyoto, Japan). The FTIR spectra were collected with 16 scans and a resolution of 2 cm^{-1}. The background spectra used for reduction were obtained at the same temperatures as that of the samples. The samples for IR measurements were prepared by drop-casting a chloroform solution of PLLA on BaF_2 windows. After the majority of the solvent had evaporated, the film was placed under vacuum at room temperature for 48 h to remove the residual solvent. Then the sample was heated to 200 °C and melted for 2 min in a Mettler FP82HT hot stage. After quenching to ~23 °C under room conditions, this sample was annealed at 40 °C for 360 h. After annealing, the sample was rapidly heated to 90 °C (or 75 °C) in the hot stage and held at this temperature for 30 min (or 180 min) for isothermal crystallization, in which process the FTIR spectra were collected at regular intervals. The isothermal crystallization of the unaged PLLA sample was also examined under the same conditions.

Polarized Optical Microscopy. Polar optical microscopic (POM) observation was performed on an BX90 polarizing optical microscope (Olympus Co., Tokyo, Japan) equipped with a digital camera. The PLLA sample sandwiched by two glass slides was heated to 200 °C and held for 2 min in a Mettler FP82HT hot stage, followed by quenching to ~23 °C to attain the amorphous sample. Then it was annealed at 40 °C for 360 h. Afterward, the aged sample was heated to 140 °C for crystallization. The spherulite morphology was recorded at different times. For comparison, the spherulite morphology of the unaged sample prepared under the same melting and quenching conditions was also observed.

Results and Discussion

Nonisothermal Crystallization Measured by DSC. The physical aging kinetics are quite dependent on the aging temperature (T_a). In the experimental study, physical aging is generally conducted at a temperature close to but below T_g.[2] In this study, the aging temperatures 40 (T_g − 15 °C) and 50 °C (T_g − 5 °C) were selected. WAXD and FTIR measurements show that the samples are amorphous after aging at 40 and 50 °C for 840 h, as expected according to the general crystallization theory. Figure 1 shows the DSC heating curves of PLLA unaged and aged at 40 °C for different periods (t_a). In addition to the glass transition (T_g) at 60 °C, all of the curves show an exothermic cold-crystallization peak (T_c) and an obvious melting peak (T_m) at higher temperature.

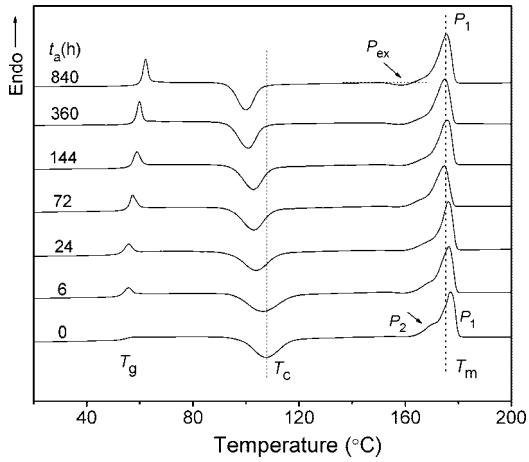

Figure 1. DSC curves, recorded upon heating at 10 °C/min, of PLLAs annealed at 40 °C for the aging periods (t_a, in hours) indicated on each curve.

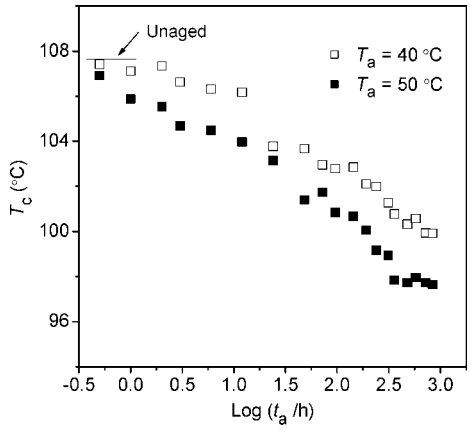

Figure 2. Dependence of cold-crystallization temperature (T_c) of PLLAs annealed at 40 and 50 °C on log t_a (aging time, in hours) derived from the DSC heating curves shown in Figure 1.

As shown in Figure 1, because of the enthalpy relaxation, the glass transition peak increases in magnitude and shifts to higher temperature progressively with aging time. With increasing t_a, the cold-crystallization peak becomes sharp and gradually shifts to lower temperature. This indicates that the crystallization rate is enhanced with aging. Besides, it can be seen that the melting behavior of PLLA slightly changes after aging. As far as the unaged PLLA is concerned, a peak shoulder, denoted as P_2, is present on the low-temperature side of the major melting peak (P_1). With increasing t_a, the peak shoulder P_2 decreases in magnitude and disappears gradually. Meanwhile, an exotherm (P_{ex}) appears prior to the dominant melting peak, which can be distinctly observed for the sample aged for 840 h. The difference between melting behavior could be attributable to the effect of crystallization temperatures, which has been reported to affect the crystalline structure of PLLA.[17]

For the samples aged at 50 °C, a very similar trend was observed in the DSC traces (data not shown). To quantitatively analyze the aging effect on the cold-crystallization behavior, the crystallization temperature (T_c) in the heating process was evaluated and plotted against the logarithm of t_a (log t_a, in hours) in Figure 2. As seen in Figure 2, the T_c value decreases nearly linearly with log t_a in the investigated t_a region. Additionally, as T_a increases, the T_c value decreases, reflecting that the aging-induced enhancement in the crystallization rate becomes more distinct at higher T_a because of the faster relaxation and reorganization of the polymer chains (which is restricted in the quenching process).

Table 1. Kinetic Parameters of Isothermal Cold-Crystallization at 90 °C for PLLAs Unaged and Aged at 40 °C for Various t_as Calculated from DSC Results[a]

t_a (h)	$t_{1/2}$ (min)	ΔH_c (J/g)	n	k (min^{-n})
0	4.03	−28.2	2.42	0.024
24	2.58	−26.9	2.37	0.074
144	1.95	−28.1	2.55	0.125
240	1.77	−27.2	2.61	0.156
360	1.59	−27.9	2.58	0.210

[a] t_a, aging time; $t_{1/2}$, crystallization half-time; ΔH_c, crystallization enthalpy; n, Avrami index, k, overall rate constant.

Isothermal Crystallization Measured by DSC. Aging effects on isothermal crystallization behavior were examined by DSC. Figure 3 shows the DSC curves of isothermal cold-crystallization at 90 °C and the subsequent melting for PLLA unaged and aged at 40 °C for various times t_a. As shown in Figure 3a, with increasing t_a, the crystallization peak becomes sharp and the peak time (t_p), corresponding to the time when the exotherm minimum occurs, decreases obviously. This further indicates that crystallization is accelerated by the aging process. As shown in Figure 3b, no appreciable change in the position or shape of the melting peaks is observed. For all the samples with different thermal histories, an exotherm (P_{ex}), is present prior to the major melting peak (P_1), which is characteristic for PLLA crystallized at lower temperatures (<100 °C).[17] This implies that the variation in melting behavior with aging shown in Figure 1 is ascribed to the effect of crystallization temperature.

The well-known Avrami equation[11b] is frequently employed to analyze the isothermal crystallization of polymer, and its linear form is given as follows:

$$\log [-\ln (1 - X_t)] = \log k + n \log t \quad (1)$$

where X_t is the relative degree of crystallinity at a given time t, which can be calculated from the integrated area of the DSC curve from $t = 0$ to $t = t$ divided by the integrated area of the whole heat flow curve. n is the Avrami index and k is the overall rate constant. The crystallization half-time $t_{1/2}$, which is defined as the time when X_t arrives at 50%, can be determined from the X_t vs t plot.

The parameters of crystallization kinetics, together with the crystallization enthalpy (ΔH_c), for unaged and aged PLLAs are summarized in Table 1. The crystallization half-time ($t_{1/2}$, panel a) and peak time (t_p, panel b) of PLLAs aged at 40 and 50 °C are plotted as a function of log t_a (in hours) in Figure 4. As shown in Table 1 and Figure 4, the $t_{1/2}$ value decreases with aging. The Avrami rate constant k increases remarkably with increasing t_a. With aging at 40 °C for 360 h, the values of $t_{1/2}$ and k are respectively ~39% and 875% of those of the unaged PLLA. These again indicate that the crystallization rate increases with aging. Analogously to the results shown in Figure 2, the $t_{1/2}$ and t_p values decrease nearly logarithmically with t_a in the investigated T_a region, as seen in Figure 4. This is similar to the reported results that the yield strength, tensile modulus, and enthalpy loss (in the glass transition region) of amorphous polymers vary almost logarithmically with aging time.[4b,7a] However, it should be noted that these relationships between kinetics parameters T_m, $t_{1/2}$, t_p, and aging time are just empirical proposals, and the theoretical relationships between them are still unclear. Besides, the $t_{1/2}$ value of PLLA aged at 40 °C is smaller than that of PLLA aged at 50 °C for the identical period, further suggesting that the aging effect on the crystallization becomes more distinct with increasing T_a.

Isothermal Crystallization Examined by Time-Resolved FTIR Spectroscopy. Isothermal crystallization behavior was also investigated for both unaged and aged PLLAs by time-resolved FTIR spectroscopy. Figure 5a shows the time-resolved FTIR spectra in the 1850−1000 cm^{-1} region for unaged PLLA

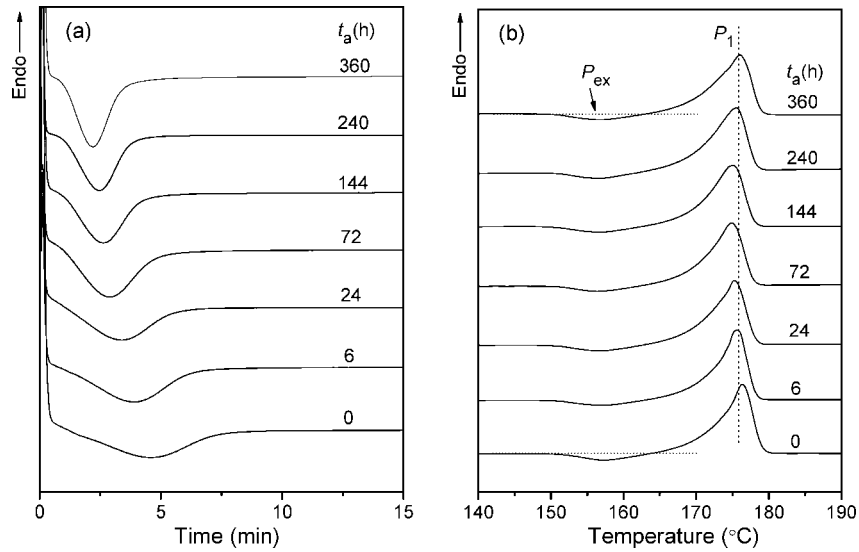

Figure 3. DSC curves of (a) isothermal cold-crystallization and (b) subsequent heating scans at 10 °C/min for PLLAs annealed at 40 °C for the aging periods (t_a, in hours) indicated on each curve.

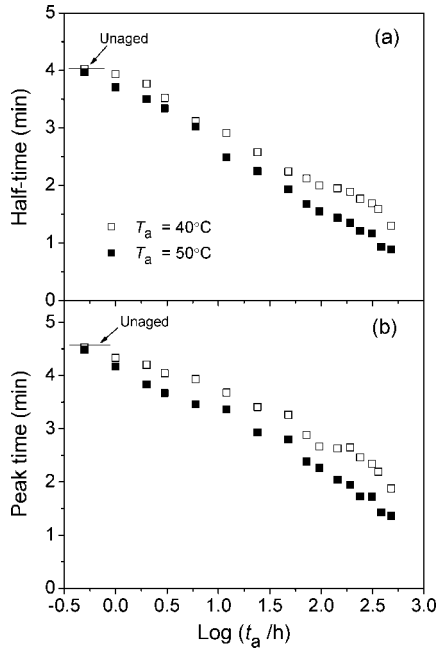

Figure 4. Dependence of (a) crystallization half-time ($t_{1/2}$) and (b) peak time (t_p) on log t_a (aging time, in hours) for PLLAs aged at 40 and 50 °C.

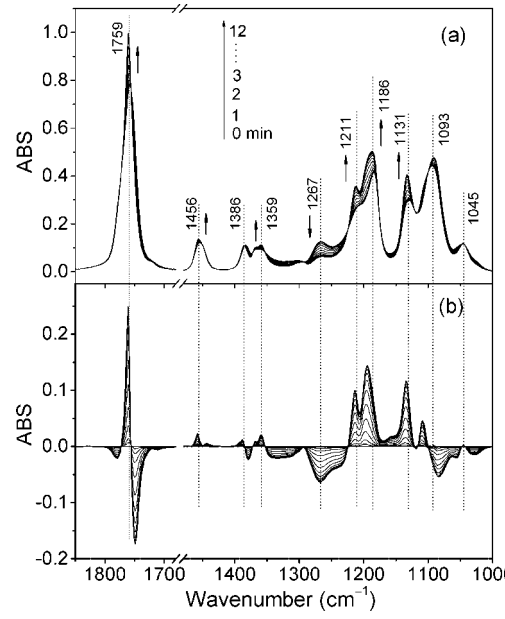

Figure 5. (a) Time-resolved FTIR spectra in the 1850−1000 cm^{-1} region of unaged PLLA isothermally cold-crystallizing for time t = 0∼12 min at 90 °C. (b) Difference spectra at crystallization time t = 0∼12 min, obtained by subtraction of the initial spectrum at t = 0 from the spectra shown in panel a.

isothermally cold-crystallizing at 90 °C. A similar trend of change, albeit with different kinetics, is observed for the sample aged at 40 °C for 360 h (data not shown). The bands in the 1850−1700 and 1500−1300 cm^{-1} regions have been assigned to the C═O stretching vibration [ν(C═O)], CH_3 and CH bending vibration [$\delta(CH_3)$ and δ(CH)], and the 1300−1000 cm^{-1} range is mainly ascribed to the coupling of the C−O−C backbone stretching [ν(C−O−C)], CH_3 rocking [r(CH_3)], and δ(CH) vibration modes.[16a,b] During the course of crystallization, absorbencies of the crystalline-sensitive bands increase while those of the amorphous-dependent bands decrease. By subtracting the initial spectrum from the consecutive spectra, difference spectra can be achieved, as shown in Figure 5b, in which the FTIR bands of the PLLA crystalline and amorphous phases overlap severely in the range of 1850−1000 cm^{-1}. In order to quantitatively analyze the kinetics, bands of pure crystalline or amorphous phases are necessary.

Figure 6 shows the time-resolved spectra in the 1000−800 cm^{-1} region, which is sensitive to the degree of crystallinity,[16d] for the unaged and aged (at 40 °C for 360 h) PLLA isothermally cold-crystallizing at 90 °C. Peak shifting and intensity changes can be observed during the crystallization process. The bands at 922 and 956 cm^{-1} are ascribed respectively to the crystalline phase in the PLLA α (or α′) form with a 10_3 helix conformation and to the amorphous phase, arising from the coupling of C−C backbone stretching [ν(C−COO)] and the CH_3 rocking mode [r(CH_3)].[16a,b] As seen in Figure 6, at the initial stage of crystallization of the two samples, no peak can be observed at nearby 922 cm^{-1}, suggesting the absence of crystallinity. In the course of crystallization, the peak intensity at 922 and 956 cm^{-1} respectively increases and decreases monotonously without shifting. Thus the 922 and 956 cm^{-1} bands were considered as the pure crystalline- and amorphous-specific bands, respectively. The band at ∼870 cm^{-1}, attributed to the C−C backbone

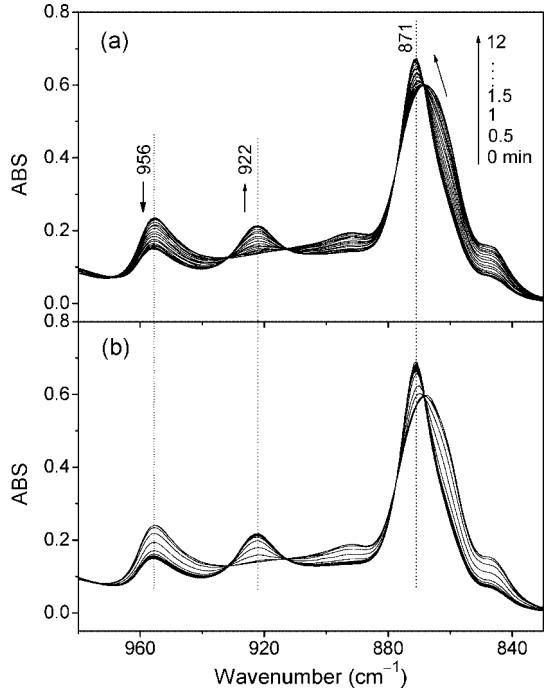

Figure 6. (a) Time-resolved FTIR spectra in the 980−830 cm^{-1} range for (a) unaged and (b) aged (at 40 °C for 360 h) PLLAs isothermally cold-crystallizing at 90 °C.

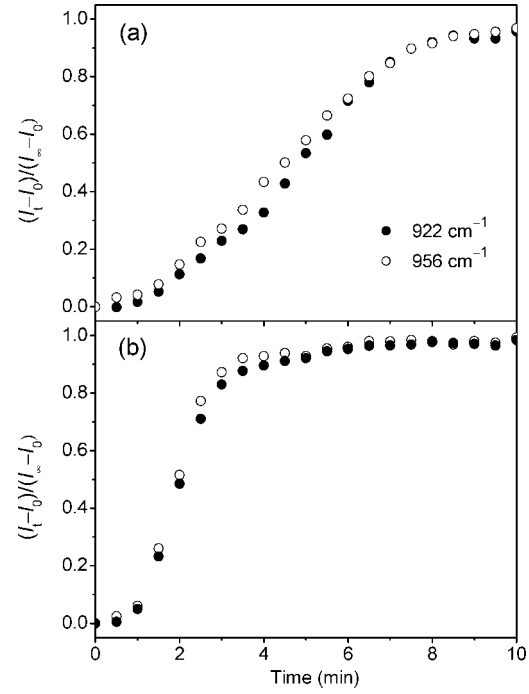

Figure 7. Normalized peak intensity of the bands at 922 and 956 cm^{-1} as a function of crystallization time for (a) unaged and (b) aged (at 40 °C for 360 h) PLLAs isothermally cold-crystallizing at 90 °C.

stretching [ν(C−COO)], shifts to higher wavenumbers and becomes sharper in the crystallization process, suggesting a transition to an ordered structure.

To qualitiatively analyze the crystallization kinetics, the peak intensities were normalized as follows:

$$X_{\mathrm{IR},t} = (I_t - I_\infty)/(I_0 - I_\infty) \quad (2)$$

where $X_{\mathrm{IR},t}$ is the relative degree of crystallinity derived from FTIR results. I_t is the peak intensity at crystallization time t. I_∞ and I_0 are respectively the peak intensities at completion of crystallization and at $t = 0$. In the isothermal cold-crystallization at 90 °C, I_∞ corresponds to the peak intensity recorded at t = 30 min. The normalized intensities of the bands at 922 and 956 cm^{-1} are plotted as a function of crystallization time in Figure 7 for the (a) unaged and (b) aged (at 40 °C for 360 h) PLLA. By comparing panels a and b of Figure 7, it is obvious that the crystallization rate increases with aging.

The time-resolved FTIR results were further analyzed on the basis of eqs 1 and 2. The estimated parameters of crystallization kinetics are summarized in Table 2. As shown in Table 2, similar to the kinetics parameters attained from DSC measurements, the $t_{1/2}$ value decreases and the k value increases with aging. It should be noted that the kinetics parameters derived from the two measurements are not completely identical. This could be due to the fact that the crystallization conditions in the FTIR and DSC measurements are somewhat different. In the former case, the film sample crystallizes on the BaF_2 surface, whereas in the latter case, the bulk sample crystallizes in a sealed aluminum pan. Furthermore, as shown in Figure 7, the bands at 922 and 956 cm^{-1} do not vary synchronously, and at the same crystallization time, the normalized intensity change of the 956 cm^{-1} band is slightly larger than that of the 922 cm^{-1} one. Also, the $t_{1/2}$ value derived from the 956 cm^{-1} band is smaller than that estimated from the 922 cm^{-1} counterpart (see Table 2). These will be discussed in the following sections.

Spherulite Morphology. The effects of physical aging on the spherulite morphology during the cold-crystallzation were

Table 2. Kinetic Parameters of Isothermal Cold-Crystallization at 90 °C for PLLAs Unaged and Aged at 40 °C for Various t_as Estimated from FTIR Results[a]

	band at 922 cm^{-1}			band at 956 cm^{-1}		
samples	$t_{1/2}$ (min)	n	k (min^{-n})	$t_{1/2}$ (min)	n	k (min^{-n})
unaged	4.84	2.64	0.011	4.49	2.31	0.021
aged	2.03	2.40	0.109	1.97	2.58	0.117

[a] $t_{1/2}$, crystallization half-time; n, Avrami index; k, overall rate constant.

observed by POM. Because the spherulite is too small to be clearly discerned in the crystallization at T_c = 90 °C, a higher T_c, that is, 140 °C, was chosen in this measurement. Figure 8 shows the POM micrographs of the unaged and aged (at 40 °C for 360 h) PLLA after cold-crystallizing at 140 °C for t = 2, 10, and 30 min. At t = 30 min, the crystallization of both samples finishes. As shown in Figure 8, the nuclei number of the aged sample is remarkably larger than that of the unaged counterpart crystallized for the same time. Comparing images c and c′ in Figure 8, it is obvious that the nucleation density is larger and spherulite size is smaller in the aged sample than those in the unaged counterpart at the completion of crystallization. For the unaged and aged PLLA cold-crystallized at T_c = 90 °C, the spherulite morphology was also observed by scanning electron microscopy (SEM) after the erosion of the samples in 1 M aqueous solution of sodium hydroxide for 72 h. The SEM images (data not shown) also show that the spherulite size decreases and nucleation density increases with aging. These results strongly suggest that the nucleating ability of PLLA is highly improved with physical aging. It is reasonable to conclude that the aging-induced acceleration in PLLA crystallization is due to the enhanced nucleation.

Induction Period of Crystallization. In order to clarify the origin and mechanism for physical aging effects on crystallization behavior, the crystallization induction period of PLLA with and without aging was investigated. Because the cold-crystallization of PLLA at T_c = 90 °C is relatively faster, a lower temperature, that is, T_c = 75 °C, was selected to study the crystallization induction period. Figure 9 shows the DSC curves

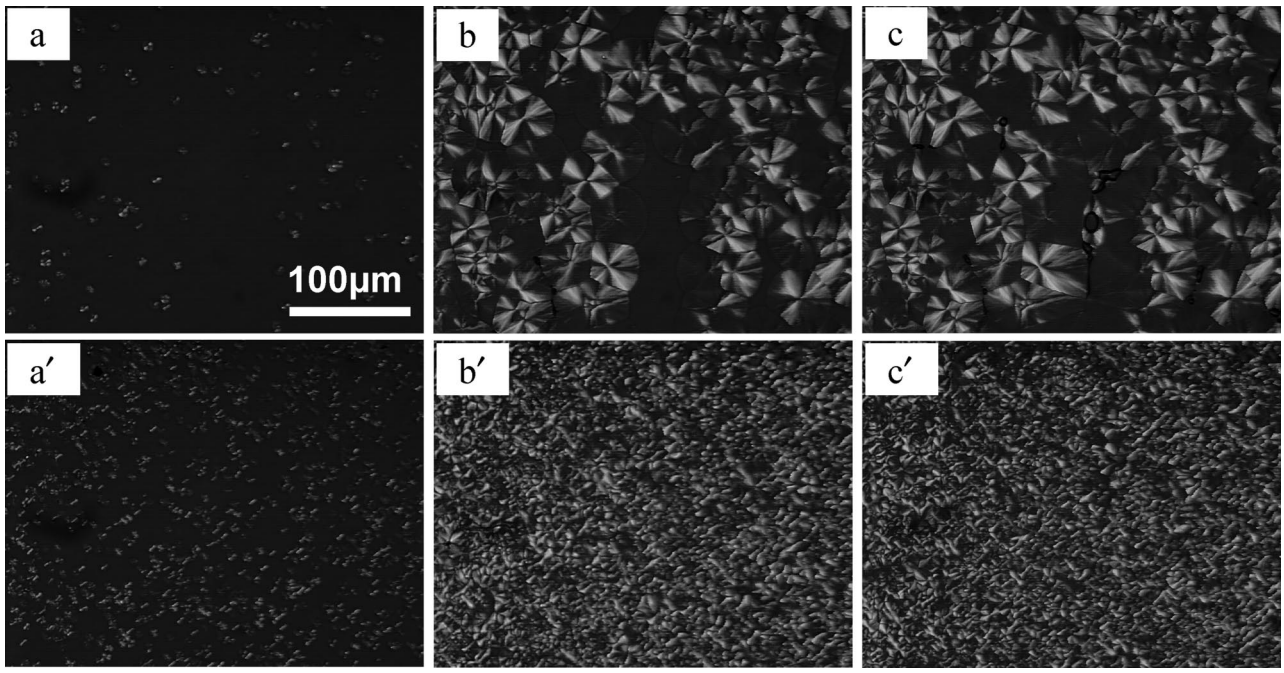

Figure 8. POM micrographs of PLLAs: (a−c) unaged and (a′−c′) aged at 40 °C for 360 h after isothermal cold-crystallization at 140 °C for (a, a′) 2 min, (b, b′) 10 min, and (c, c′) 30 min.

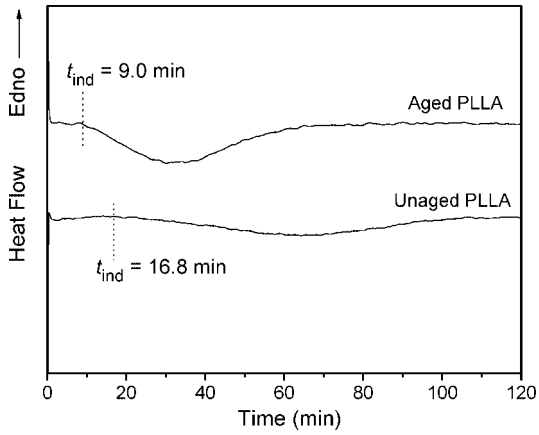

Figure 9. DSC curves of isothermal cold-crystallization at 75 °C for PLLAs unaged and aged at 40 °C for 360 h.

of isothermal cold-crystallization at 75 °C for PLLA unaged and aged at 40 °C for 360 h. The induction period (t_{ind}) was taken as the onset time of the crystallization peak. It was estimated that, with aging at 40 °C for 360 h, the t_{ind} value decreases to ∼9.0 min from ∼16.8 min of the unaged sample. As seen in Figure 9, the crystallization time decreases with aging.

The induction periods during cold-crystallization at 75 °C were also investigated for aged and unaged PLLA by time-resolved FTIR spectroscopy. The peak intensities were normalized according to eq 2, where I_∞ is the peak intensity collected at t = 180 min. Figure 10 shows the normalized intensity changes of 922 and 956 cm^{-1} bands for the (a) unaged and (b) aged (at 40 °C for 360 h) PLLA. The intensity changes in the crystallization induction period were enlarged and shown as the insets in Figure 10. By comparison of panels a and b of Figure 10, it can be clearly seen that for aged PLLA the crystallization process is faster and it takes a relatively shorter time for crystallizing.

The conformational state and conformer distribution of PLLA have been studied by several authors.[16c,18] According to the

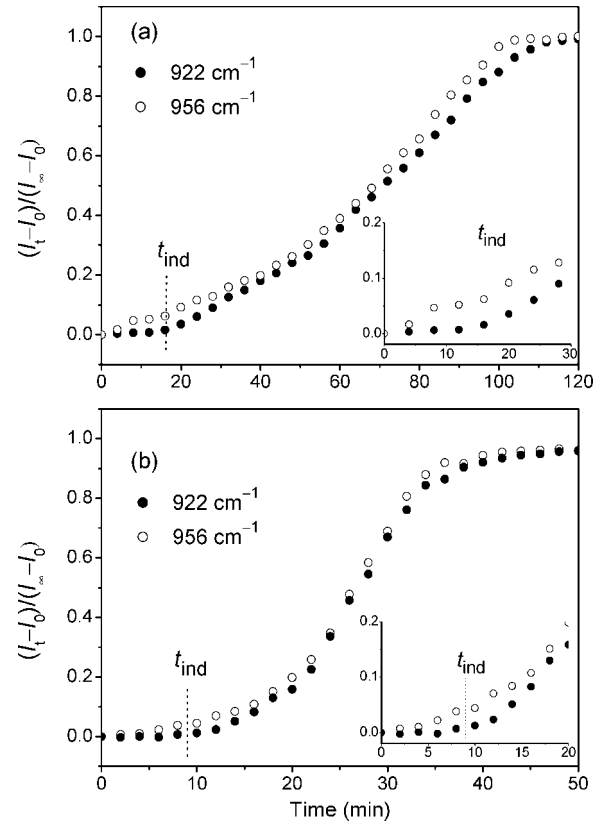

Figure 10. Normalized peak intensity of the bands at 922 and 956 cm^{-1} as a function of crystallization time for (a) unaged and (b) aged (at 40 °C for 360 h) PLLAs isothermally cold-crystallizing at 75 °C. (Insets) Enlarged graphs for the initial stage of the crystallization process.

rotational isomeric state (RIS) model and associated conformational map, it has been found that there are two dominant conformations in PLLA, the most energy-favorable *gt* (10_3 or 3_1 helix) and second energy-favorable *gg* (4_1 helix), where *t* and *g* denote the trans and gauche conformations, respec-

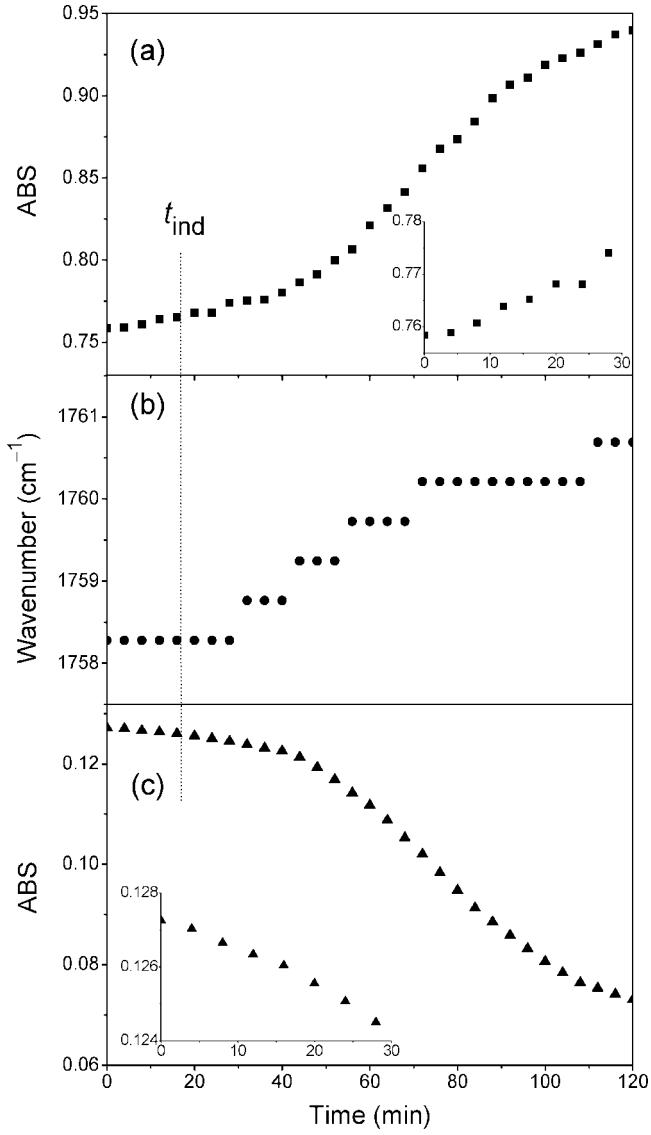

Figure 11. (a) Intensity and (b) peak wavenumber of the C═O stretching vibration band, and (c) peak intensity of 1267 cm^{-1} band as a function of crystallization time for unaged PLLA isothermally cold-crystallizing at 75 °C. (Insets) Enlarged graphs for the initial stage of the crystallization process.

tively.[16c,18] On the basis of the calculated contour map, it has been suggested that at room temperature in a completely random structure of PLLA the content of these two major conformers is more than 90%.[18a] Previous study[16c] has reported that the ν(C═O) vibration mode is very sensitive to the conformational state and the distribution of conformer population of PLLA. Besides, in our previous study[7b] on the glass transition behavior of PLLA, it was found that the ν(C−O−C) vibration region in the FTIR spectra is also sensitive to the conformational state of PLLA, and the 1267 cm^{-1} band has been assigned to be more sensitive to the ν_{as}(C−O−C) + δ(CH) vibration mode of the less energy-favorable *gg* conformers of PLLA.

To study the conformational behavior of PLLA in the crystallization induction period, the intensity changes of conformation-sensitive bands, that is, ν(C═O) and 1267 cm^{-1}, were monitored. Figure 11 shows the (a) intensity and (b) wavenumber changes of the ν(C═O) band, and (c) the intensity change of the 1267 cm^{-1} band for unaged PLLA crystallizing at 75 °C. The insets in Figure 11a,c present the intensity changes of the corresponding bands at the early stage of crystallization. As for the aged PLLA, with the exception of the kinetics, very similar variation trends in the intensities and wavenumber were observed (data not shown). As shown in Figure 11, the ν(C═O) band increases in intensity and shifts to the higher-wavenumber side, and the 1267 cm^{-1} band intensity decreases during the crystallization process.

Similar to the results shown in Figure 7, the intensities of 922 and 956 cm^{-1} bands shown in Figure 10 do not vary synchronously for both unaged and aged samples. As seen in the insets of Figure 10, the intensity of the 922 cm^{-1} band, which is a pure crystalline band and sensitive to helix formation in the PLLA crystalline phase, shows almost no change in the induction period. This indicates that the crystalline phase is nearly not formed in the induction period. However, in the case of the 956 cm^{-1} band, attributed to the ν(C−C) + r(CH$_3$) vibration of PLLA in the amorphous phase, the intensity change can be clearly observed in the induction period. Similarly, the intensities of ν(C═O) and 1267 cm^{-1} bands start to vary (see insets of Figure 11a,c) during the crystallization induction period. As shown in Figure 11b, no shift in the ν(C═O) band wavenumber is observed in the induction period, which is possibly due to the fact that the crystalline phase is almost not generated and the structural change is relatively small at this stage.

As shown in Figures 10 and 11, the intensity changes in the 956 cm^{-1}, ν(C═O), and 1267 cm^{-1} bands precede that of the 922 cm^{-1} counterpart in the early stage of crystallization, which is in accordance with previous studies.[13d,16a] On the basis of FTIR measurements, Krikorian and Pochan[16a] have detected that the change in normalized intensity of the 922 cm^{-1} band is much slower than that of skeletal conformation-sensitive bands signified by the 1207 and 1458 cm^{-1} peaks in the early stage of PLLA crystallization. They suggested that the chain conformational adjustment in entangled amorphous phase precedes helix formation in the ordered crystalline region. Besides, through studying the crystallization process of poly(bisphenol A-*co*-decane ether) by using FTIR spectroscopy, Jiang et al.[13d] observed that the intensity change in the crystalline bands shows a time lag compared with that of the conformation-sensitive bands and thus suggested that the intramolecular conformational changes occur some time before the formation of crystal lattice. Therefore, it is reasonable to consider that the microstructural and/or conformational changes in amorphous PLLA possibly occur in the crystallization induction period.

Unlike traditional polymers such as PET[9a] or isotactic and syndiotactic polystyrene,[13a,b] the conformation-sensitive bands in the FTIR spectrum of PLLA have not been clearly assigned at present. In this study the conformational behavior of PLLA in the crystallization process was only qualitatively analyzed on the basis of the FTIR results. As shown in Figure 11a,c, the intensities of these two conformation-sensitive bands changing during the crystallization induction period shows a similar trend as that observed in the crystal formation (including nucleation and crystal growth) stage, suggesting that the adjustment of chain conformation possibly occurs in a similar manner during these two stages (induction period and crystal formation). Since the PLLA chain adopts a *gt* conformation (10_3 helix) in the crystalline phase of the α (or α′) form,[16a,c,17] it can be expected that the *gg* conformers rearrange into the *gt* couterparts in the crystal formation process. The decrease in intensity of 1267 cm^{-1} band (see Figure 11c) also indicates that the *gg* conformer content decreases in the induction period, according to the previous assignment.[7b] Therefore, it is considered that the conformational rearrangement from *gg* to *gt* occurs in the crystallization induction period prior to the crystal formation process. This conclusion is also supported by the results reported by Kaji and co-workers.[13a] By analyzing the conformational bands of syndiotactic polystyrene by time-resolved FTIR measurements,

Kaji and co-workers[13a] found that the gauche conformation converts into the trans counterpart not only in the crystal formation stage but also in the induction period, accompanying the chain extension.

Correlation between Physical Aging and Crystallization Induction Period. In our previous paper,[7b] it has been evidenced by FTIR measurements that the less energy-favorable *gg* conformers of PLLA rearrange into the more energy-favorable *gt* counterparts during physical aging. This is similar to the conformational changes occurring in the crystallization induction period. Besides, Roe and co-workers[14a,b] have observed density fluctuation by X-ray scattering methods and suggested that the local ordered domain is formed during the physical aging of polymers. This conclusion is also supported by our previous finding that that the distribution of ^{13}C spin−lattice relaxation rate broadens with physical aging.[7b] As described in the Introduction, formation of long-range ordered structure has also been observed by many authors via different analysis methods.[8−10] These suggest that the conformational and microstructural changes occurring in the two processes, that is, physical aging and crystallization induction period, might be similar. In the quenched polymer, packing of the frozen chains is disordered and contains many conformational defects such as entanglements, sharp folds, or chain torsion, which might obstruct the nucleation formation and diffusion of polymer chain in the subsequent crystallization process.[8a] Because the chain conformation and microstructure readjust to the more energy-favorable state from the entangled chain state during aging, it takes a relatively shorter time for the aged sample to perform the conformational and/or microstructural rearrangements before nucleation and crystal growth in the subsequent cold-crystallization process. For this reason, the crystallization induction period of PLLA decreases and the nucleation process becomes faster with aging.

As discussed above, the initial states of polymer, especially those related to chain packing and conformation, are the key factors governing the crystallization process. On the other hand, in the past several decades it has been widely reported that the shear flow in the polymer melt can accelerate crystallization.[11b] Many in situ and ex situ experiments have shown that the shear flow promotes local chain alignment and chain conformational ordering and generates the nanodomains with an intermediate degree of order that is usually referred to as crystal nucleation precursors.[19] From this viewpoint, it is proposed that the physical aging effect on crystallization is somewhat like that of shear flow, and the local ordering domains formed during physical aging could possibly act as nucleation precursors in the subsequent crystallization process. More work should be conducted in the future to verify this proposal.

Conclusions

The effects of physical aging on the crystallization kinetics and induction period have been investigated by DSC, POM, and FTIR measurements. Nonisothermal and isothermal crystallization results have revealed that the cold-crystallization rate is considerably enhanced with aging. The crystallization temperature in the heating process and the half-time in isothermal crystallization decrease approximately logarithmically with t_a in the investigated t_a region. With increasing T_a, the aging effect on crystallization becomes more distinct. POM observation signifies that the aging-induced enhancement in crystallization rate is because of the improved nucleation ability. Besides, it is found that the crystallization induction period is shortened with physical aging. FTIR results suggest that the conformational rearrangement likely occurs in the crystallization induction period. The aging-induced enhancement in the crystallization rate of PLLA can be correlated with conformational and microstructural rearrangements taking place during the aging process, which are considered to be similar to those occurring in the crystallization induction period.

Acknowledgment. We thank Dr. Kazue Ueda of Unitika Co. Ltd. (Kyoto, Japan) for kindly supplying PLLA sample.

References and Notes

(1) (a) Darder, M.; Aranda, P.; Ruiz-Hitzky, E. *Adv. Mater.* **2007**, *19*, 1309–1319. (b) Nair, L. S.; Laurencin, C. T. *Prog. Polym. Sci.* **2007**, *32*, 762–798.
(2) (a) Hutchinson, J. M. *Prog. Polym. Sci.* **1995**, *20*, 703–760. (b) Hodge, I. M. *J. Non-Cryst. Solids* **1994**, *169*, 211–266.
(3) (a) Jansssen, R. P. M.; de Kanter, D.; Govaert, L. E.; Meijer, H. E. H. *Macromolecules* **2008**, *41*, 2520–2530. (b) Klompen, E. T. J.; Engels, T. A. P.; Govaert, L. E.; Meijer, H. E. H. *Macromolecules* **2005**, *38*, 6997–7008. (c) van Melick, H. G. H.; Govaert, L. E.; Raas, B.; Nauta, W. J.; Meijer, H. E. H. *Polymer* **2003**, *44*, 1171–1179. (d) Klompen, E. T. J.; Engels, T. A. P.; van Breemen, L. C. A.; Schreurs, P. J. G.; Govaert, L. E.; Meijer, H. E. H. *Macromolecules* **2005**, *38*, 7009–7017.
(4) (a) McGonigle, E. A.; Daly, J. H.; Jenkins, S. D.; Liggat, J. J.; Pethrick, R. A. *Macromolecules* **2000**, *33*, 480–489. (b) Hutchinson, J. M.; Smith, S.; Horne, B.; Gourlay, G. M. *Macromolecules* **1999**, *32*, 5046–5061.
(5) (a) Laot, C. M.; Marand, E.; Schmittmann, B.; Zia, R. K. P. *Macromolecules* **2003**, *36*, 8673–8684. (b) Huang, Y.; Paul, D. R. *Macromolecules* **2005**, *38*, 10148–10154.
(6) (a) McGonigle, E. A.; Daly, J. H.; Gallagher, S.; Jenkins, S. D.; Liggat, J. J.; Olsson, I.; Pethrick, R. A. *Polymer* **1999**, *40*, 4977–4982. (b) Lu, X.; Hay, J. N. *Polymer* **2000**, *41*, 7427–7436. (c) Tan, S.; Su, A.; Luo, J.; Zhou, E.; Cheng, S. Z. D. *Macromol. Chem. Phys.* **1999**, *200*, 2487–2493. (d) Sánchez, F. H.; Mateo, J. M.; Colomer, J. R.; Sánchez, M. S.; Ribelles, J. L. G.; Mano, J. F. *Biomacromolecules* **2005**, *6*, 3283–3290.
(7) (a) Pan, P.; Zhu, B.; Inoue, Y. *Macromolecules* **2007**, *40*, 9664–9671. (b) Pan, P.; Zhu, B.; Dong, T.; Yazawa, K.; Inoue, Y.; Shimizu, T.; Tansho, M. Submitted for publication.
(8) (a) Imai, M.; Kaji, K.; Kanaya, T. *Macromolecules* **1994**, *27*, 7103–7108. (b) Imai, M.; Mori, K.; Mizukami, T.; Kaji, K.; Kanaya, T. *Polymer* **1992**, *33*, 4451–4456. (c) Imai, M.; Kaji, K.; Kanaya, T. *Phys. Rev. Lett.* **1993**, *71*, 4162–4165. (d) Imai, M.; Kaji, K.; Kanaya, T.; Sakai, Y. *Phys. Rev. B* **1995**, *52*, 12696–12704.
(9) (a) Radhakrishnan, J.; Kaito, A. *Polymer* **2001**, *42*, 3859–3866. (b) Nogales, A.; Ezquerra, T. A.; Denchev, Z.; Baltá-Calleja, F. J. *Polymer* **2001**, *42*, 5711–5715.
(10) (a) Shimada, T.; Doi, M.; Okano, K. *J. Chem. Phys.* **1988**, *88*, 2815–2821. (b) Doi, M.; Shimada, T.; Okano, K. *J. Chem. Phys.* **1988**, *88*, 4070–4075. (c) Shimada, T.; Doi, M.; Okano, K. *J. Chem. Phys.* **1988**, *88*, 7181–7186.
(11) (a) Strobl, G. R. *Eur. Phys. J. E* **2000**, *3*, 165–183. (b) Strobl, G. R. *The Physics of Polymers*; Springer-Verlag; Berlin, 2007; pp 163−222.
(12) (a) Fukao, K.; Miyamoto, Y. *Phys. Rev. Lett.* **1997**, *79*, 4613–4616. (b) Takeuchi, H. *J. Chem. Phys.* **1998**, *109*, 5614–5621.
(13) (a) Matsuba, G.; Kaji, K.; Nishida, K.; Kanaya, T.; Imai, M. *Macromolecules* **1999**, *32*, 8932–8937. (b) Zhang, J.; Duan, Y.; Shen, D.; Yan, S.; Noda, I.; Ozaki, Y. *Macromolecules* **2004**, *37*, 3292–3298. (c) Kimura, T.; Ezure, H.; Tanaka, S.; Ito, E. *J. Polym. Sci., Polym. Phys.* **1998**, *36*, 1227–1233. (d) Jiang, Y.; Gu, Q.; Li, L.; Shen, D. Y.; Jin, X. G.; Chan, C. M. *Polymer* **2004**, *44*, 3509–3513. (e) Lee, D. H.; Park, K. H.; Kim, Y. H.; Lee, H. S. *Macromolecules* **2007**, *40*, 6277–6282.
(14) (a) Roe, R. J.; Curro, J. J. *Macromolecules* **1983**, *16*, 428–434. (b) Song, H. H.; Roe, R. J. *Macromolecules* **1987**, *20*, 2723–2732.
(15) (a) Soloukhin, V. A.; Brokken-Zijp, J. C. M.; van Asselen, O. L. J.; de With, G. *Macromolecules* **2003**, *36*, 7585–7597. (b) Heymans, N. *Polymer* **1997**, *38*, 3435–3440. (c) Lu, J.; Wang, Y.; Shen, D. *Polym. J.* **2000**, *32*, 610–615. (d) Wang, Y.; Shen, D.; Qian, R. *J. Polym. Sci., Polym. Phys.* **1998**, *36*, 783–788.
(16) (a) Krikorian, V.; Pochan, D. J. *Macromolecules* **2005**, *38*, 6520–6527. (b) Kister, G.; Cassanas, G.; Vert, M. *Polymer* **1998**, *39*, 267–273. (c) Meaurio, W.; Zuza, E.; López -Rodríguez, N.; Sarasua, J. R. *J. Phys. Chem. B* **2006**, *110*, 5790–5800. (d) Meaurio, E.; López-Rodríguez, N.; Sarasua, J. R. *Macromolecules* **2006**, *39*, 9291–9301.
(17) (a) Pan, P.; Kai, W.; Zhu, B.; Dong, T.; Inoue, Y. *Macromolecules* **2007**, *40*, 6898–6905. (b) Zhang, J.; Tashiro, K.; Tsuji, H.; Domb, A. J. *Macromolecules* **2008**, *41*, 1352–1357. (c) Yasuniwa, M.; Sakamo, K.; Ono, Y.; Kawaharam, W. *Polymer* **2008**, *49*, 1943–1951.
(18) (a) Brant, D. A.; Tonelli, A. E.; Flory, P. J. *Macromolecules* **1969**, *2*, 228–235. (b) Kang, S.; Hsu, S. L.; Stidham, H. D.; Smith, P. B.; Leugers, M. A.; Yang, X. *Macromolecules* **2001**, *34*, 4542–4548. (c)

Yang, X.; Kang, S.; Hsu, S. L.; Stidham, H. D.; Smith, P. B.; Leugers, A. *Macromolecules* **2001**, *34*, 5037–5041.

(19) (a) Azzurri, F.; Alfonso, G. C. *Macromolecules* **2008**, *41*, 1377–1383. (b) An, H.; Zhao, B.; Ma, Z.; Shao, C.; Wang, X.; Fang, Y.; Li, L.; Li, Z. *Macromolecules* **2007**, *40*, 4740–4743. (c) Somani, R. H.; Yang, L.; Hsiao, B. S.; Agarwal, P. K.; Fruitwala, H. A.; Tsou, A. H. *Macromolecules* **2002**, *35*, 9096–9104. (d) Kumaraswamy, G.; Kornfield, J. A.; Yeh, S.; Hsiao, B. S. *Macromolecules* **2002**, *35*, 1762–1769. (e) Byelov, D.; Panine, P.; de Jeu, W. H. *Macromolecules* **2007**, *40*, 288–289.

MA801436F